Structure of ordered and disordered α-brass

S. Müller and Alex Zunger
National Renewable Energy Laboratory, Golden, Colorado 80401
(Received 14 June 2000; published 5 February 2001)

Alloys of copper and zinc (brass) have been widely used since Neolithic times due to the discovery that unlike regular copper this alloy can be worked ''cold'' around a 3:1 copper-to-zinc ratio. While it is now known that the as-grown system is a disordered fcc solid solution, no 3:1 ordered phase has yet been directly observed even though the negative mixing enthalpy of the disordered alloy suggests ordering tendencies. Moreover, neutron scattering experiments have been deduced that this disordered alloy contains peculiar chains of Zn atoms. We have expressed the first-principles calculated total energy of general Cu-Zn fcc-lattice configurations using a mixed-space cluster expansion. Application of Monte Carlo–simulated annealing to this generalized Ising-like Hamiltonian produces the predicted low-temperature ground state as well as finite-temperature phase diagram and short-range order. We find (i) that at low temperature the disordered fcc alloy will order into the DO_{23} structure, (ii) the high-temperature short-range order in close agreement with experiment, and (iii) chains of Zn atoms in the [001] direction, as seen experimentally. Furthermore, our model allows a detailed study of the influence and importance of strain on the phase stability.

DOI: 10.1103/PhysRevB.63.094204 PACS number(s): 61.66.Dk, 61.43.Bn, 64.70.Kb, 71.15.Ap

I. INTRODUCTION

Alloys of copper and zinc (brass) have been widely used since Neolithic times when accidental mixing of copper and zinc ores was probably the reason for the discovery of its malleability, ductility, and ability to process even in cold conditions.[1–3] While it has been historically long known[3] that above 45% Zn (''white brass'') the alloy is not workable either hot or cold, at lower Zn concentrations brass is malleable. Near 50% Zn we have the phase now known[4] to have the disordered bcc structure (β-brass) above $\sim$460 °C and the ordered CsCl structure at lower temperatures. Between 45% and 38% Zn we have the brass that can be worked only in hot conditions and is not very ductile, but is rather strong. This brass (currently used widely for manufacturing of decorative faucets) is now known as orthorombic 9R structure which can be formally derived from a face-centered tetragonal structure by introducing stacking faults on each third plane.[5] Below 38% Zn we have the historically most-widely used form of brass[1] that has excellent ''cold working'' properties and is ductile. This ''α-brass,'' which is the subject of this paper, is now known[4] to have at high temperatures the disordered fcc structure. Since it is known that the disordered bcc alloy (β) orders at low temperatures, it has long been suspected[6] that the disordered fcc alloy (α) will also order at lower temperatures. However, the ordered phase (which we might term α') was never detected, possibly due to a low order-disorder transition temperature $T_c^{\alpha\alpha'}$.

Although we know that α-brass is a disordered fcc alloy, there are definite clues that suggest that it is not a *random* alloy. First, measurements[7–9] of the mixing enthalpy of the alloy show that it is negative, suggesting the tendency of the Cu and Zn atoms to order crystallographically below some temperature $T_c^{\alpha\alpha'}$. Thus, immediately above this temperature one might expect nonrandom disorder. Second, measurements of the diffuse neutron scattering[10] of a sample quenched from high temperature ($T > T_c^{\alpha\alpha'}$) exhibit definitive deviations from randomness, manifested by peaks of the scattering around the $\langle 1\frac{1}{4}0\rangle$ and symmetrically equivalent positions in the Brillouin zone. Such peaks suggest that the disordered alloy is developing nonrandom composition waves which could signal its propensity to order crystallographically at lower temperatures. It is clear, however, from the short-range order (SRO) pattern that the structure that is being developed near $Cu_{0.75}Zn_{0.25}$ composition is *not* one of the fcc-ordered structures at the A_3B composition; for example, it is *not* the $L1_2$ structure characteristic of, e.g., Cu_3Au, Ag_3Mg, $AlPt_3$, or the DO_{22} structure characteristic of, e.g., $TiAl_3$, Ni_3V, Pd_3V. Finally, Reinhard *et al.*[10] noted that the high-temperature structure of their disordered alloy consists of unusual [001] chains with three to five Zn atoms whose abundance exceeds that expected from a random alloy. These too suggest a propensity for some ordering.

A number of attempts have been made to theoretically predict the structure of α- and α'-brass. Hume-Rothery[6] has noted that Cu-Zn belongs to a class of compounds whose structure correlates with the electron-per-atom (e/a) ratio. The basic concept is that alloys between the $d^{10}s^1$ noble metals (Cu, Ag, Au) and elements to the right of them in the periodic table (i.e., $d^{10}s^xp^y$ elements with full d bands) occur at characteristic electron per atom ratios.[11] In these systems the d band of the solute atoms lies far below the Fermi level and thus its influence on the Fermi electrons diminishes on alloying. During alloying the kinetic energy of the free electrons is lowered due to the formation of a gap in the Brillouin zone boundary by the introduction of an extra period characteristic of the ordered formed compound. Since this mechanism depends only on the valence electrons, the structure formed is uniquely defined by e/a.

Following this idea, Sato and Toth[12] showed in 1961 that if one considers a superlattice $(L1_2)_M/(L1_2)'_M$ of period M made of the $L1_2$ and a displaced $L1_2$ cell as candidate structures for Cu_3Zn, then the period M is given by the e/a ratio and the ratio t between the actual Fermi-surface diameter along (110) and the diameter of an equivalent free-electron Fermi surface. If the peak of the measured[10] SRO can be

interpreted as an image of the Fermi surface along (110), then according to Reinhard *et al.*[10] $t=0.94$. Using this value and $e/a=1.25$ yields, using the Sato-Toth model, the ground-state structure with period $M\sim 2$. While highly suggestive, such Hume-Rothery concepts focus but on one piece of the total energy of the solid (the sum $\Sigma_i^{\epsilon_F}\epsilon_i$ of single-particle energies up to the Fermi level), neglecting interelectronic (Coulomb, exchange, and correlation) and ionic terms. Also, the atomic size-mismatch-induced strain (encoded in the full total energy) is neglected. It is important to emphasize that this approach does not predict the stable structure (out of many possible candidate configurations), but rather assumes it at the outset. Already early experimental studies[13,14] found deviations from ideal Hume-Rothery behavior in Cu-Zn; e.g., Mössbauer investigations[13] reported a stronger increase in the electron density of α-brass (fcc solid solution) than in that of β-brass (CsCl structure), when pressure is applied, while according to the Hume-Rothery rules the opposite should be true, because the number of outer electrons per atom is higher in β- than in α-brass.

More quantitative attempts to predict the structure of α- and α'-brass were carried out recently. Johnson *et al.*[15] were able in 1986 [with further details given in 1990 (Ref. 16)] to calculate the total energy of perfectly random alloys using the full (local-density) total energy expression, rather than the $\Sigma_i^{\epsilon_F}\epsilon_i$ single-particle term alone used by Hume-Rothery[6] and by earlier practitioners of the coherent potential approximation (CPA).[17,18] Johnson *et al.* were able to calculate the equilibrium lattice parameter of fcc-disordered $Cu_{1-x}Zn_x$ (finding a small deviation from Vegard's rule) and a mixing enthalpy of $\Delta H(Cu_{0.65}Zn_{0.35})=-55$ meV/atom, compared with the measured value $\Delta H=-82$ meV/atom.[4,5] No attempt was made to introduce SRO effects in the description of the random alloy or to predict the ordered low-temperature phase. Since this calculation neglected atomic displacements, assumed a spherical muffin-tin approximation to the atomic potential, and, as was latter discovered,[19] omitted unwitingly the ion-ion Madelung interactions, the accuracy was limited. Subsequently, Johnson and Pinski[20] added the previously missing[15,17,18] Madelung term, finding that $\Delta H(Cu_{0.65}Zn_{0.35})$ changes from -55 meV/atom to -80 meV/atom, in much better agreement with experiment.

A rather complete theoretical study of the phase stability of Cu-Zn alloys was conducted by Turchi *et al.*[21,22] They use the perfectly random alloy (as modeled via the CPA) as a starting point for a perturbative expansion of the energy. The unperturbed CPA energy was given just by the single-particle term $\Sigma_i\epsilon_i$ without interelectronic Coulomb, exchange, and correlation, or Madelung terms, while the perturbation about the CPA medium was expressed as an Ising-type cluster expansion over (composition-dependent) pair-only interactions. Atomic displacements and the ensuring elastic strain energy were neglected. Despite these simplifications the authors were able to calculate a realistic SRO diffuse scattering map, the phase diagram and the fcc mixing enthalpy $\Delta H(Cu_{0.65}Zn_{0.35})=-53$ meV/atom. Because of the limited accuracy, the stable structure obtained for Cu_3Zn at $T=0$ was $L1_2$,[21] which is inconsistent with the measured[10] SRO. Nevertheless, the calculated SRO of Turchi *et al.*[21,22] signaled the propensity of developing at lower temperature some long-periodic superstructures.

Given that the questions of the structure of disordered (α) and ordered (α') phases of brass are yet-unsolved fundamental problems in alloy theory, we attempt here a solution. We use an approach that incorporates in a natural manner the presently recognized factors that affect alloy stability. The total energy is described via the local-density approximation (LDA), including both single-particle ($\Sigma_i\epsilon_i$) as well as interelectronic and interionic terms. Charge-transfer (Madelung) and energy-lowering atomic displacements are fully included. The configurational degrees of freedom representing arbitrary degrees of deviations from randomness are treated via a Monte Carlo simulation of the above-mentioned energy functional. To facilitate intensive Monte Carlo samplings, we expand our energy functional in an Ising-like series, so that the energy of each configuration can be rapidly computed. Such cluster expansion formalism,[23–25] generalized by Sanchez, Ducastelle, and Gratias,[23] allows, e.g., a fast and reliable ground-state search in a huge parameter space with quantum-mechanical accuracy. Our mixed-space cluster expansion[25] (MSCE) casts the $T=0$ LDA configurational energy (used by the $T\neq 0$ Monte Carlo simulations) as a linear series in both pairwise and many-body terms, designed to accurately reproduce the directly calculated LDA total energies of simple-ordered configurations.

The main results of the application of our MSCE method to fcc Cu-Zn alloys are the following: (i) The low-temperature ordered phase is identified as the DO_{23} structure. The order-disorder transition temperature is $T=140$ K at $x_{Zn}=0.10$ and $T=295$ K at $x_{Zn}=0.33$. (ii) The high-temperature SRO scattering exhibits $\langle 1\frac{1}{4}0\rangle$ peaks, in close agreement with the neutron experiment of Reinhard *et al.*[10] (iii) Real-space imaging of our short-range order exhibits [001] chains of Zn atoms in the disordered phase, as seen experimentally. (iv) The calculated alloy mixing enthalpy with SRO is in close agreement with experiments, e.g., $\Delta H(x=0.3,\ T=773\ \mathrm{K})=-81.1$ meV/atom compared with the measured value of -77.8 meV/atom, and predicts a temperature dependence: Short-range order leads to a strong decrease in the mixing enthalpies of the alloy. (v) We described the impact of the previously neglected strain energy on the phase-stability and finite-temperature properties, finding that without strain terms the mixing enthalpies of the random alloy are up to about 20% too low and the order-disorder transition temperatures are about 20 K higher than those obtained from calculations including strain.

II. METHOD

In the MSCE,[25] any configuration σ is defined by specifying the occupations of each of the N lattice sites by a Cu atom (spin index $\hat{S}_i=-1$) or a Zn atom ($\hat{S}_i=+1$). The formation enthalpy of any configuration σ at its atomically relaxed state is conveniently given by

$$\Delta H_{CE}(\sigma)=E_{pair}(\sigma)+E_{many-body}(\sigma)+E_{CS}(\sigma). \quad (1)$$

The first term $E_{pair}(\sigma)$ includes *all* pair figures, where $J_{pair}(\mathbf{k})$ and $S(\mathbf{k},\sigma)$ are lattice Fourier transforms of real-space interactions and spin-occupation variables:

$$E_{pair}(\sigma)=\sum_{\mathbf{k}} J_{pair}(\mathbf{k})|S(\mathbf{k},\sigma)|^2. \tag{2}$$

The second sum $E_{many\text{-}body}(\sigma)$ includes many-body interactions and runs over symmetry-inequivalent clusters consisting of three or more lattice sites:

$$E_{many\text{-}body}(\sigma)=\sum_{f}^{MB} D_f J_f \overline{\Pi}_f(\sigma). \tag{3}$$

Here, D_f is the number of equivalent clusters per lattice site, and $\overline{\Pi}_f(\sigma)$ are structure-dependent geometrical coefficients (spin products). These first two terms include all the information about strength and importance of different chemical interactions characterized by effective cluster interactions J_{pair} and J_f. It does not consider the energy necessary to maintain coherency between the Cu and fcc Zn matrix caused by the lattice misfit. This part is considered in the last term $E_{CS}(\sigma)$:

$$E_{CS}(\sigma)=\frac{1}{4x-1}\sum_{\mathbf{k}} \Delta E^{eq}_{CS}(\hat{k},x)|S(\mathbf{k},\sigma)|^2. \tag{4}$$

This term involves the *constituent strain energy* ΔE^{eq}_{CS}, which is defined as the strain energy of bulk Cu and fcc Zn required to maintain coherency along an interface with orientation $\hat{k}$. For this, the bulk elements (Cu and fcc Zn) are deformed from their equilibrium lattice constants a_{Cu} and a_{Zn} to a common lattice constant a perpendicular to $\hat{k}$. Then, $\Delta E_{CS}(\sigma)$ is given by expanding $\Delta E^{eq}_{CS}(x,\hat{k})$ as[26]

$$\Delta E_{CS}(\sigma)=\sum_{\mathbf{k}} J_{CS}(x,\hat{k})|S(\mathbf{k},\sigma)|^2, \tag{5}$$

with

$$J_{CS}(x,\hat{k})=\frac{\Delta E^{eq}_{CS}(x,\hat{k})}{4x(1-x)}. \tag{6}$$

Consequently, ΔE^{eq}_{CS}, and therefore $E_{CS}(\sigma)$, does not include information about the strength of chemical interactions between Al and Zn atoms, but is a function of composition x and direction $\hat{k}$ only.[27]

For each configuration σ (designated by the spin values on each lattice site), it is possible to readily calculate $\overline{\Pi}_f(\sigma)$, D_f, and $S(\mathbf{k},\sigma)$. Given these three quantities, as well as the $\Delta E^{eq}_{CS}(x,\hat{k})$ obtained from simple LDA calculations on end-point compounds, the unknowns in Eqs. (2)–(4) are $J_{pair}(\mathbf{k})$ and J_f. These are obtained by fitting a set $\{\Delta H_{LDA}(\sigma_s);s=1,\ldots,N_s\}$ of directly calculated LDA formation enthalpies for N_s ordered configurations σ_s to the cluster-expansion expression $\Delta H_{CE}(\sigma)$. The formation enthalpy $\Delta H_{LDA}(\sigma)$ of an ordered A_pB_q bulk compound is defined as the energy gain or loss with respect to the bulk constituents at their equilibrium lattice constants:

$$\Delta H_{LDA}(\sigma)=E^{tot}(A_pB_q,\sigma)-xE^{tot}_A(a_A)-(1-x)E^{tot}_B(a_B). \tag{7}$$

Here, a_A and a_B are the equilibrium lattice constants of the bulk elements A and B, and $E^{tot}_A(a_A)$ and $E^{tot}_B(a_B)$ are the total energies of A and B, respectively. As shown earlier (see, e.g., Refs. 28, 26, and 29), it is essential that the calculated formation enthalpies correspond to the *geometrically fully relaxed configuration*; i.e., the structures have to be optimized (consistent with the symmetry of the structure) with respect to unit cell vectors, cell-internal atomic displacements, and the volume of the unit cell.

We obtain $\Delta H_{LDA}(\sigma_s)$ using the pseudopotential total-energy and force method.[30] The pseudopotentials were generated using the prescription of Troullier and Martins.[31] The exchange correlation term was treated by the local-density approximation of Ceperley and Alder[32] in the parametrization of Perdew and Zunger.[33] A plane-wave basis with kinetic energy cutoff of 80 Ry and a total of $12\times12\times12$ equivalent k points[34] is necessary to converge the formation enthalpies. The pseudopotentials were carefully tested and successfully used in an earlier work on Al-Cu and Al-Zn (for details, see Ref. 35).

We have computed ΔH_{LDA} for $N_s=23$ ordered structures defined by their composition and layer orientation in Fig. 1. Fitting these energies to our expansion of Eq. (1) yields $\{J_{pair}(\mathbf{k})\}$ and $\{J_f\}$. Structures marked by an asterisk in Fig. 1 were not used for the fit, but represent actual predictions. The average prediction error (1.63 meV/atom) is also shown on the top of Fig. 1. The unusually small maximum error of 2.3 meV/atom [prediction of $\Delta H(Y2)$] permits us to study in detail the delicate energy balance being essential for our ground-state search (see Sec. III A).

Once we have a converged cluster expansion, we can calculate the $T=0$ ground state and the finite-temperature SRO by using our cluster-expansion Hamitonian in Monte Carlo (MC) simulations. The SRO behavior of the system for a given temperature and concentration can be quantified in terms of Warren-Cowley SRO parameter which will be described in Sec. III E. For the ground-state search, we anneal a randomly generated configuration for a given concentration starting with a temperature high above (here $T_{start}=700$ K) the coherent phase boundary. When equilibrium is reached, the temperature is reduced by a certain amount (typically 10 K steps). The procedure is repeated as long as spin flips take place between Cu and Zn atoms. The resulting crystal structure at $T\rightarrow0$ gives the ground state of the system. We repeated carefully the process using different MC cells and number of MC steps per temperature, as well as different temperature grids for the annealing process. This kind of ground-state search is not restricted to formation enthalpies calculated directly via the LDA, but scans about 10^{15600} of different configurations. This technique has the advantage that the ground state is not only identified by its correlation functions which we store for the final configurations, but also by the real-space atomic arrangement. Thus, there are no ambiguities as to what is the final stable structure.

Cluster-Expansion of Cu-Zn (α-brass): 21 input structures

Average fit error (CE, 21 structures): 0.12 meV
Average prediction error (4 predictions*): 1.63 meV
Maximum error: 2.30 meV

Stoich.	x_{Zn}	Direction (100)	(110)	(111)	(201)	(311)	others	others
Cu direct: CE:	0.0						fcc 0.0 -0.1	
Cu_8Zn	0.111						Ni_8Nb_a -43.9 -43.5	
Cu_7Zn	0.125						$D7$ -39.1 -39.3	
Cu_4Zn	0.20						$D1_a^*$ -66.2 -68.4	
Cu_3Zn	0.25	$Z1$ -50.4 -50.4	$Y1$ -62.7 -62.8	$V1$ -32.9 -33.0	$D0_{22}a$ -77.1 -77.1	$W1$ -63.8 -63.7	$L1_2$ -87.4 -87.3	
Cu_6Zn_2	0.25						$D023a$ -88.1 -88.0	$SQS14a$ -55.0 -55.0
Cu_9Zn_3	0.25						$LPS3a$ -87.2 -87.4	$LPS21a^*$ -85.6 -85.9
Cu_2Zn	0.333	$\beta1$ -76.9 -77.0	$\gamma1$ -92.3 -92.4	$\alpha1$ -49.0 -49.0				
$CuZn$	0.50	$L1_0$ -116.0 -115.9		$L1_1$ -83.1 -83.1				
Cu_2Zn_2	0.50	$Z2^*$ -86.6 -84.9	$Y2^*$ -66.2 -63.9	$V2^*$ -70.8	$CH(40)$ -112.6 -112.6	$W2$ -103.7 -103.7	$SQS8a$ -89.0 -89.0	$SQS8b^*$ -82.0
Zn	1.00						fcc 0.0 0.0	

FIG. 1. Cluster expansion fit for α-brass. The compounds are sorted by superlattice direction and composition. Compounds marked by an asterisk are not input structures of the cluster expansion fit, but represents predictions. While the ''average fit error'' gives the standard deviation of cluster expansion formation enthalpies of input structures, the ''average prediction error'' represents the standard deviation of all predicted structures. The ''maximum error'' is the largest deviation between the cluster expansion and LDA values.

III. RESULTS

A. $T=0$ ground-state structure of fcc $Cu_{0.75}Zn_{0.25}$

Figure 2 shows the lowest-energy structure obtained by MC-simulated annealing of our LDA energy functional of Eq. (1), out of about $10^{15\,600}$ possible configurations. The structure can be identified as DO_{23} (Cu_6Zn_2), also pointed out by Reinhard *et al.*[10] and Turchi *et al.*[21] This structure is described in Table I. It can be viewed as a superlattice between $L1_2$ and a translated $L1_2$ structure ($L1_2'$), shown in Fig. 3: DO_{23} can be constructed from $L1_2$ by forming an antiphase boundary after every two lattice constants in [001] direction; i.e., the modulation period M of the structure with respect to $L1_2$ is $M=2$. This modulation wavelength can be noted by viewing our ground-state structure as shown in the lower part of Fig. 2. Table II compares the pair- and multibody-correlation functions found by our ground-state search and those for an ideal DO_{23} structure. They are identical, proving that the found ground-state structure is indeed DO_{23}. This predicted structure was not observed experimentally as an ordered phase in Cu_3Zn, presumably because it disorders at low temperatures (see Sec. III D).

B. Energetic stability of the $T=0$ ground state and its competing structures

Our calculation reveals delicate energy balance between the various Cu_3Zn competing phases:

$$M=0,\ \Delta H(\text{random})=-55.0\ \text{meV/atom},$$
$$M=1,\ \Delta H(\text{DO}_{22})=-77.1\ \text{meV/atom},$$
$$M=2,\ \Delta H(\text{DO}_{23})=-88.1\ \text{meV/atom},$$
$$M=3,\ \Delta H(\text{LPS3})=-87.2\ \text{meV/atom},$$
$$M=\infty,\ \Delta H(L1_2)=-87.4\ \text{meV/atom}. \quad (8)$$

We see that the energy difference between DO_{22} ($M=1$) and $L1_2$ ($M=\infty$) amounts to only 11 meV/atom. Turchi

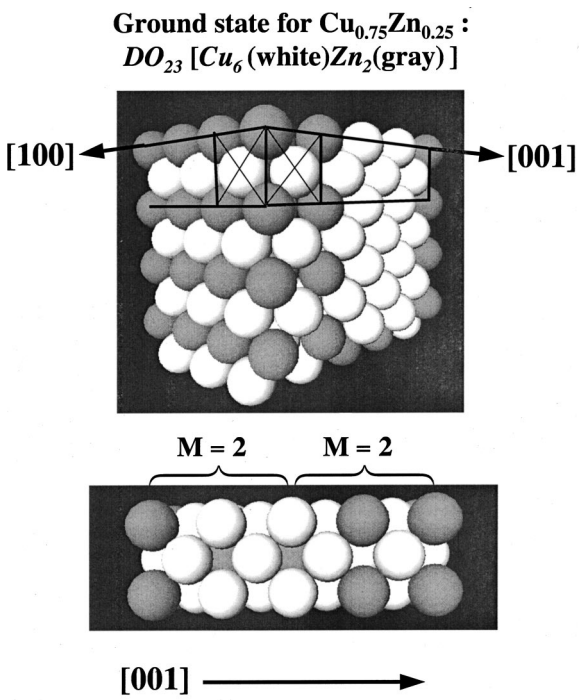

FIG. 2. Result of the ground-state search by Monte Carlo annealing: The found ground state represents a perfect DO_{23} superlattice which can be, e.g., identified by a modulation wavelength of $M=2$ between antiphase boundaries along [001].

et al.[21,22] used the lowest order in the generalized perturbation method (GPM) to calculate the energy difference between the simplest LPS, DO_{22}, and $L1_2$. The model was restricted to six pair interactions and no multibody interactions were taken into account, leading to an energy difference of about 24 mJ/m^2 (Ref. 22) between $L1_2$ and DO_{22}. Our corresponding LDA value is 22.8 mJ/m^2, in excellent agreement with the GPM result.

Since the formation enthalpies for $M=2,3$, and ∞ are all within 1 meV/atom, it is important to observe how this energy balance comes about from the qualitative physics. Figure 4(a) shows the spin products $\overline{\Pi}_i(\sigma)$ for the various pair

TABLE I. Number of nearest neighbors, distance (in units of fcc lattice constants), and number of neighbor pairs consisting of different chemical species for $L1_2$, DO_{22}, DO_{23}, and LPS3 structures.

Neighbor	Total number of neighbor atoms	Distance (a)	Number of B atoms around A			
			$L1_2$	DO_{22}	DO_{23}	LPS3
First	12	$1/\sqrt{2}$	12	12	12	12
Second	6	1	0	2	1	1
Third	24	$\sqrt{3/2}$	24	16	20	20
Fourth	12	$\sqrt{2}$	0	8	4	4
Fifth	24	$\sqrt{5/2}$	24	24	24	24
Sixth	8	$\sqrt{3}$	0	8	4	4
Seventh	48	$\sqrt{7/2}$	48	48	48	48
Eighth	6	2	0	0	2	1

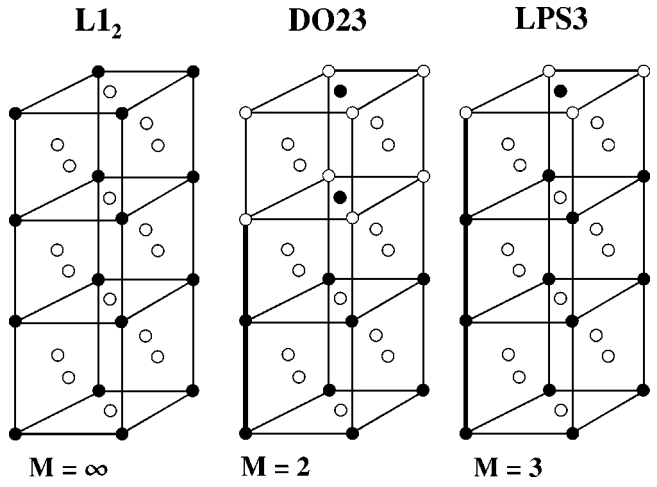

FIG. 3. Schematical pictures of the compounds $L1_2$ (Cu_3Zn), DO_{23} (Cu_6Zn_2), and LPS3 (Cu_9Zn_3). The latter two long-periodic superlattices can be constructed from $L1_2$ by antiphase boundaries parallel to [001] with modulation wavelength $M=2$ and $M=3$, respectively.

figures of the structures $M=2$, 3, and ∞. We see that (i) for the $i=1,5,9,15$ order pairs, the correlation functions $\overline{\Pi}_i(M=2)=\overline{\Pi}_i(M=3)=0$, so pair interactions of this type do not distinguish the $M=2$ from $M=3$ structure; (ii) for $i=$ even, we have $\Pi_i(M=\infty)=1$, so these pairs do contribute to $L1_2$; (iii) all other pair interactions, starting from $i=2$ can distinguish the structures $M=2$, 3, and ∞. Figure 4(b) shows the real-space pair energies J_i^{pair}. We see that for $i=1$ (nearest neighbor) the interaction is strongly ''antiferromagnetic'' (Cu-Zn attraction), while for $i=2$, 3, it is strongly ''ferromagnetic'' (Cu-Zn repulsion). We also see that regarding long-range ($i>3$) pair interactions, $i=5,6,8,10$ have the largest magnitude. In Sec. III F, we will see that the ''ferromagnetic'' interaction $i=5$ and the ''antiferromagnetic'' interaction $i=8$ are responsible for the creation of Zn chains along the [001] direction in disordered Cu-Zn fcc alloys. Figure 5(a) shows the contribution $D_i\Pi_i^{pair}J_i^{pair}$ of the ith pair to the total energy difference E_M-E_∞ between either $M=2$ (DO_{23}) or $M=3$ (LPS3) and the reference $M=\infty$ ($L1_2$) structure [horizontal line in Fig. 5(a)]. We see that the curves for $M=2$ and $M=3$ show an oscillatory behavior. However, most of the shells lead to negative energy differences with respect to $M=\infty$ and therefore to a preference of DO_{23} and LPS3 over $L1_2$. The only exceptions are shell Nos. 2 and 11. Because of this oscillatory behavior of E_M-E_∞ with the shell index i, it takes many shells to establish a clear energetic winner. Thus, six pairs[21,22] may not be sufficient to describe the physical properties of the system correctly. This is demonstrated in Fig. 5(b) that shows the *accumulative* effect $\Sigma_i^I D_i\ \Pi_i^{pair}J_i^{pair}$ of all pair interactions up to I on the energy difference E_M-E_∞. The first entry ($i=0$) in Fig. 5(b) describes the effect of the many-body terms alone, which are seen to prefer $M=3$ over $M=2$. As we add shells of pair interactions, the $M=2$ structure energies are a winner past the $I=10$th nearest-neighbor shell.

Although our search clearly finds DO_{23} as the low-

TABLE II. Pair- and multibody-correlation functions resulting from the ground-state search for $Cu_{0.75}Zn_{0.25}$ via Monte Carlo annealing. As can be seen, the values found are identical to those of DO_{23}, identifying this compound as low-temperature ground of α-brass.

PAIR-IA	$\Pi_i^{pair}(DO_{23})$	$\Pi_i^{pair}(MC)$	MB-IA	$\Pi_i^{mb}(DO_{23})$	$\Pi_i^{mb}(MC)$
J_1	0.0000	0.0000	$J3$	0.5000	0.5000
J_2	0.8333	0.8333	$K3$	−0.3333	−0.3333
J_3	0.1667	0.1667	$L3$	0.3333	0.3333
J_4	0.6667	0.6667	$M3$	−0.5000	−0.5000
J_5	0.0000	0.0000	$J4$	−1.0000	−1.0000
J_6	0.5000	0.5000	$K4$	−0.1667	−0.1667
J_7	0.1667	0.1667	$L4$	−0.8333	−0.8333
J_8	0.6667	0.6667			
J_9	0.0000	0.0000			
J_{10}	0.3333	0.3333			

temperature ground state of α-brass, the discussion above makes clear that a consideration of fewer than ten pair interactions would lead to an incorrect answer: $L1_2$ would then be the low-temperature ground state of Cu_3Zn, in disagreement with experimental SRO studies.[10] Furthermore, we see that a consideration of at least 15 pair interactions is necessary to reach convergence in the energy differences between the structures with $M=2$, $M=3$, and $M=\infty$. Actually, the consideration of such a large number of interactions distinguish our approach from earlier theoretical investigations[15,16,20–22] on α-brass.

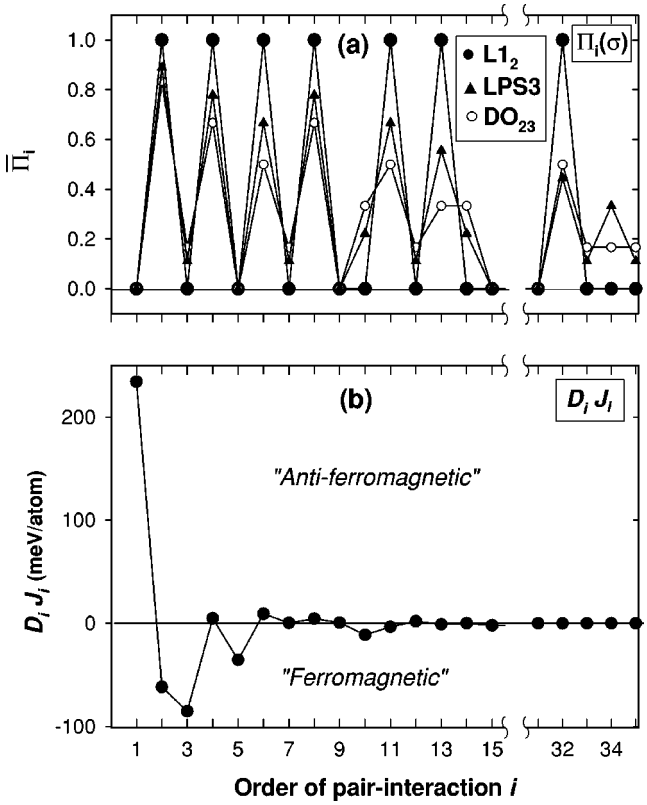

FIG. 4. (a) Pair correlation functions $\overline{\Pi}_i$ for $L1_2$ and on $L1_2$ based superlattices σ (DO_{23} and LPS3). (b) Energy value of each individual effective pair interaction J_i.

C. Comparison of $T=0$ long-period structures of Cu_3Zn and Cu_3Pd

Figure 6 compares the energies of the long-period superlattices E_M vs M for Cu_3Zn and Cu_3Pd. Values for Cu_3Pd are taken from Lu *et al.*[36] In excellent agreement with the LDA calculated formation enthalpies of Cu_3Zn (shown as open squares) our prediction locates a minimum for $M=2$, corresponding to the DO_{23} structure. Lu *et al.*[36] found for

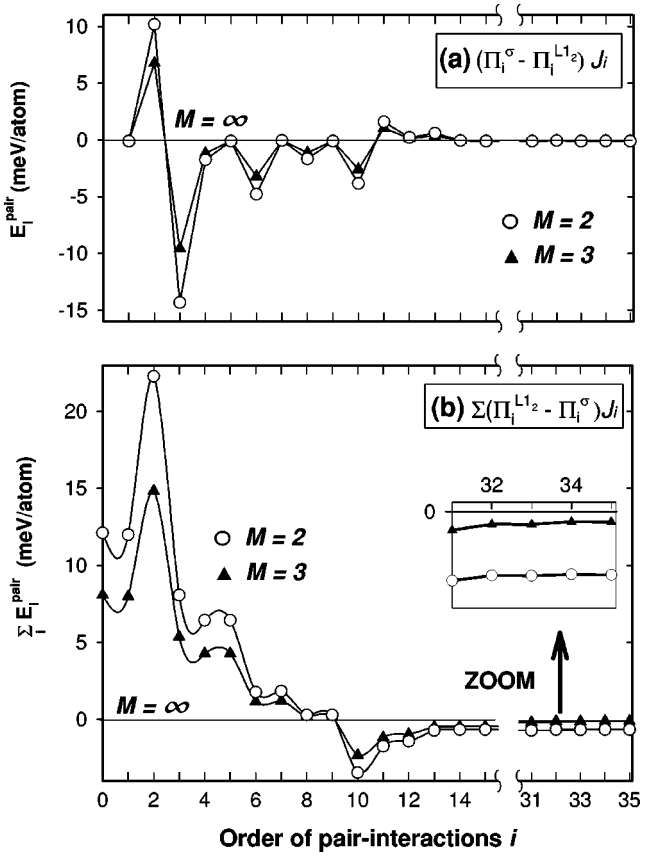

FIG. 5. Energy difference between $L1_2$ ($M=\infty$) and on $L1_2$ based superlattices σ (DO_{23}, $M=2$, and LPS3, $M=3$) as function of (a) each individual pair interactions, (b) total number of used effective pair interactions.

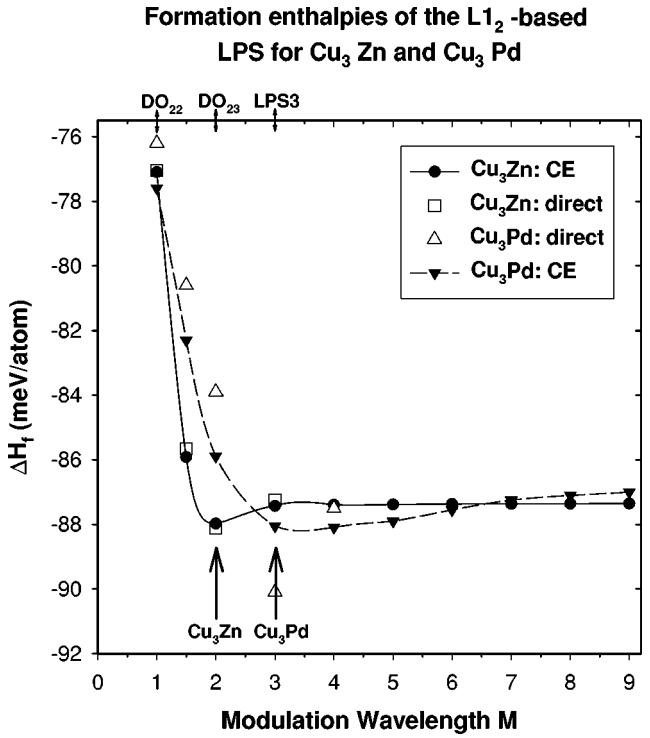

FIG. 6. Direct (LDA) and via cluster-expansion calculated formation enthalpies for the LPS group of Cu_3Zn and Cu_3Pd.

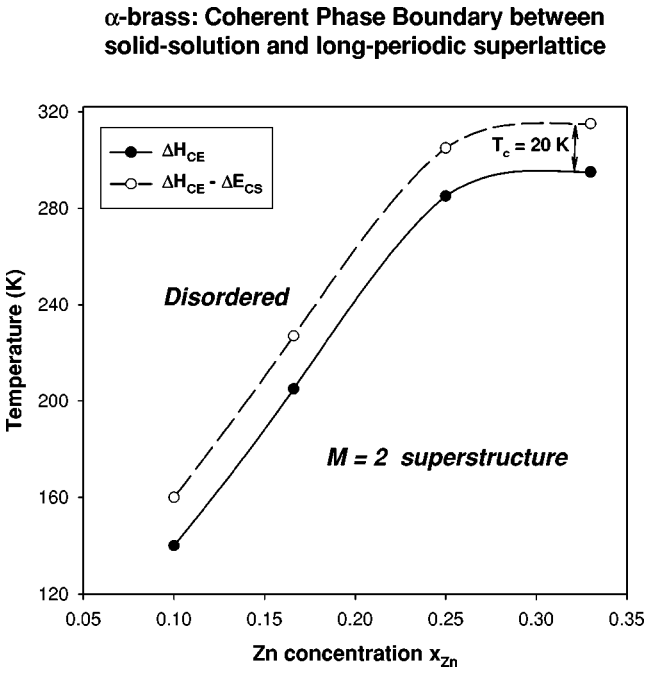

FIG. 7. Coherent phase boundary in α-brass calculated with (solid line) and without (dashed line) taking the constituent strain energy ΔE_{CS} into account.

Cu_3Pd the $M=3$ structure as the most stable structure of the LPS group. It is interesting to note that following the work by Sato and Toth,[12] a modulation wavelength $M=4$ is expected for Cu_3Pd instead of the LDA value $M=3$: The use of a ratio $t=0.94$ (already introduced in Sec. I) and $e/a=0.75$ for Cu_3Pd gives $e/a=0.70$ for $M=3$, but $e/a=0.74$ for $M=4$.

Since in Cu_3Zn the $T=0$ stable structure is $M=2$, whereas in Cu_3Pd it is $M=3$, we expect to see ''fingerprints'' of these differences on the SRO diffuse scattering. Since the fundamental reciprocal space wave vector of long-periodic superlattices is given by $\mathbf{k}=\langle 1\ 1/2M\ 0\rangle$ with M being the modulation wavelength (see, e.g., Refs. 36 and 37), SRO peaks should appear at different positions in the diffuse scattering patterns of Cu_3Zn and Cu_3Pd. While Cu_3Zn with DO_{23} ($M=2$) as ground state should show SRO intensities at $\mathbf{k}=\langle 1\frac{1}{4}0\rangle$ and symmetrtically equivalent positions (in agreement with the observation), Cu_3Pd with LPS3 ($M=3$) as ground state should show SRO intensities at $\mathbf{k}=\langle 1\frac{1}{6}0\rangle$ and symmetrtically equivalent positions. This is discussed in Sec. III E.

D. Finite-temperature boundary between the ordered low-temperature structure α' and the disordered alloy α

We next study finite-temperature effects. The solid line in Fig. 7 shows our calculated phase diagram, delineating the ordered $M=2$ superlattice from the disordered alloy. This phase boundary can be identified by Monte Carlo–simulated annealing, recording the specific heat c_V as a function of temperature. Being the response function of the energy, c_V has a maximum at the critical temperature T_c. Repeating the annealing process for different concentrations leads to the coherent phase boundary. The resulting curve is given as solid line. The important result of Fig. 7 is that T_c is very low on the scale of growth temperatures. Thus, it might be difficult to detect the ordered phase directly.

In order to study the importance of the constituent strain energy E_{CS}, Eq. (4), we switched E_{CS} off, and repeated our Monte Carlo annealing to determine T_c. The resulting curve for T_c is shown as a dashed line in Fig. 7. We see that (i) $\Delta H_{CE}-E_{CS}$ leads to about 20 K higher transitions temperatures, and (ii) the two curves are practically parallel; i.e., the temperature difference between them does not depend much on the Zn concentration. The behavior is understandable in terms of the ordering energies δE_{ord}, given by

$$\delta E_{ord}=\Delta H_{ord}-\Delta H_{rand}. \tag{9}$$

Here, ΔH_{ord} and ΔH_{rand} are the formation enthalpies, Eq. (7), of an ordered compound and a random alloy, respectively, at the same composition. As shown by Zunger *et al.*[38] the formation enthalpy of a random alloy, ΔH_{rand}, can be successfully described by quasirandom structures (called SQS structures). For the following estimation, we will use the formation enthalpy of SQS14*a* (Cu_6Zn_2) as formation enthalpy of the random alloy for $x_{Zn}=0.25$. Using our cluster-expansion Hamiltonian, Eq. (1), this leads to an ordering energy

$$\delta E_{ord}=\Delta H_{DO_{23}}-\Delta H_{SQS14a}=-33.1\ \text{meV/atom},$$

while a neglect of constituent strain energies leads to

$$\delta E_{ord(no\text{-}strain)} = [\Delta H_{DO_{23}} - E_{CS}(DO_{23})] - [\Delta H_{SQS14a} - E_{CS}(\mathrm{SQS14}a)] = -39.4 \text{ meV/atom}.$$

So neglecting strain leads to a more negative ordering energy and, therefore, to a more stable DO_{23} structure. Consequently, the coherent phase boundary will shift to higher temperatures.

E. Short-range order diffuse scattering in the high-temperature disordered α-brass

Having calculated the $T=0$ stable phase of Cu_3Zn (Fig. 2) as well as the finite temperature at which this structure disorderes (Fig. 7), we next study the properties of the disordered high-temperature phase. The (SRO) can be described in terms of the Warren-Cowley SRO parameters which are given for shell (lmn) by

$$\alpha_{lmn}(x) = 1 - \frac{P_{lmn}^{A(B)}}{x}, \tag{10}$$

where $P_{lmn}^{A(B)}$ is the conditional probability that given an A atom at the origin, there is a B atom at (lmn). The sign of α indicates qualitatively whether atoms in a given shell prefer to order ($\alpha<0$) or cluster ($\alpha>0$). The SRO parameter may be written in terms of the cluster expansion pair correlations as

$$\alpha_{lmn}(x) = \frac{\langle \overline{\Pi}_{lmn} \rangle - q^2}{1-q^2}, \tag{11}$$

where $q=2x-1$ and $\langle \overline{\Pi}_{lmn} \rangle$ is the pair correlation function for shell (lmn). In diffraction experiments the portion of diffuse scattering due to SRO is proportional to the lattice Fourier transform of $\alpha_{lmn}(x)$:

$$\alpha(x,\mathbf{k}) = \sum_{lmn}^{n_R} \alpha_{lmn}(x) e^{i\cdot\mathbf{k}\cdot\mathbf{R}_{lmn}}. \tag{12}$$

Figure 8(a) shows the measured SRO pattern for α-brass obtained from neutron diffraction studies by Reinhard *et al.*[10] The experiments were done for a Zn concentration of 31.1% Zn, being very close to the transition concentration between α- and β-brass. The experimental pattern clearly shows SRO intensities around $\mathbf{k}=\langle 1\,\frac{1}{4}\,0\rangle$. Figure 8(b) gives the corresponding calculated SRO pattern in two different presentations resulting from our calculations. For this, we used the Hamiltonian, Eqs. (1)–(4), in Monte Carlo simulations for a given Zn concentration x and temperature T. In agreement with earlier experimental work,[10] we find SRO peaks around $\langle 1\,\frac{1}{4}\,0\rangle$ (and symetrically equivalent) positions. Since the fundamental reciprocal-space wave vector of an ordered long-periodic superlattice is given by $\mathbf{k}=\langle 1\ 1/2M\ 0\rangle$ (see, e.g., Refs. 36 and 37) and $M=2$ for DO_{23} (see Fig. 3), the corresponding SRO peaks should be at $\mathbf{k}=\langle 1\,\frac{1}{4}\,0\rangle$, in agreement with observation.

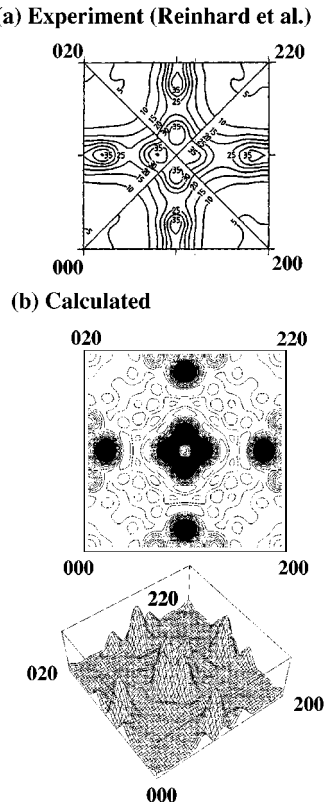

FIG. 8. Short-range order intensity pattern of α-brass for $T=473$ K and $x_{Zn}=0.31$ resulting from (a) neutron diffraction experiments (Ref. 10), (b) our MSCE. In both cases, SRO peaks around $\langle 1\,\frac{1}{4}\,0\rangle$ are visible, favoring DO_{23} as the low-temperature ground state.

For a quantitative comparison of SRO with experiment we calculated the Warren-Cowley SRO parameter α_{lmn}, Eq. (11), for the first 22 shells of a $Cu_{0.689}Zn_{0.311}$ alloy at $T=473$ K and compared our values to those obtained from neutron scattering experiments.[10] The comparison is shown in Table III. Considering the fact that the experimental error of α_{000} amounts to being already 8% and that the authors give about the same error also for all further parameters, the agreement between our predicted values and experimentally determined values is reasonable. We see that (i) α_{110} is negative, indicating that Zn atoms prefer Cu atoms as nearest neighbors, and (ii) all α_{2n00} are positive, while all $\alpha_{(2n-1)10}$ are negative.

The *concentration dependence* of the SRO intensities for the temperature above ($T=473$ K) is shown in Fig. 9. For a concentration $x_{Zn}=0.311$, this temperature is already relatively close to the critical temperature T_c ($T\approx 1.55T_c$) compared with the other concentrations in Fig. 9, so characteristic SRO peaks around $[1\,\frac{1}{4}\,0]$ become visible. Furthermore, the intensity maxima are elongated most along [100] which can be already interpreted as a hint for the observed chains of atoms.[10] With decreasing Zn concentration, this effect vanishes; however, also the ''temperature distance'' to the coherent phase boundary increases, so that SRO becomes less

TABLE III. Warren-Cowley SRO parameter α_{lmn} resulting from our parameter-free model and from experimental studies (Ref. 10) for $Cu_{0.689}Zn_{0.311}$ at $T=473$ K.

(lmn)	α_{lmn}^{expt}	α_{lmn}^{theo}
000	1.0831	1.0000
110	−0.1373	−0.1689
200	0.1490	0.1863
211	0.0196	0.0196
220	0.0358	0.0883
310	−0.0404	−0.0453
222	−0.0077	0.0371
321	−0.0036	−0.0132
400	0.0296	0.0279
330	−0.0134	−0.0211
411	0.0141	0.0306
420	0.0050	0.0825
332	−0.0005	−0.0050
422	−0.0050	−0.0050
431	0.0068	0.0148
510	−0.0107	−0.0186
521	−0.0019	−0.0092
440	−0.0050	−0.0104
433	0.0038	0.0092
530	−0.0066	−0.0057
442	−0.0084	−0.0145
600	0.0130	0.0017

important. For $x_{Zn}=0.20$, the SRO peaks are no longer exactly on $[1\frac{1}{4}0]$ positions, but are displaced to $[1\frac{1}{6}0]$. This could be a consequence of ''missing'' Zn atoms (concentration is smaller than 25%) so that on the average the modulation wavelength M has to be increased and, therefore, the SRO peaks are shifted towards the X point.

For studying the *temperature dependence* of the SRO intensities, we chose again a concentration $x_{Zn}=0.311$ and a starting temperature $T=473$ K. Intensity patterns for three different temperatures are shown in Fig. 10. Going from $T=473$ K to $T=330$ K the SRO intensity becomes more concentrated in the peaks characteristic for DO_{23}. However, we are still in the region of the solid solution in the phase diagram, i.e., *above* the corresponding critical temperature. Crossing the coherent phase boundary the long-periodic superlattice DO_{23} is formed ($T=150$ K), indicated by sharp peaks at $[1\frac{1}{4}0]$ and symetrically equivalent peaks.

Figure 11 compares for $x_{zn}=0.20$ the SRO pattern calculated by Turchi *et al.*[21] using the concentration wave method

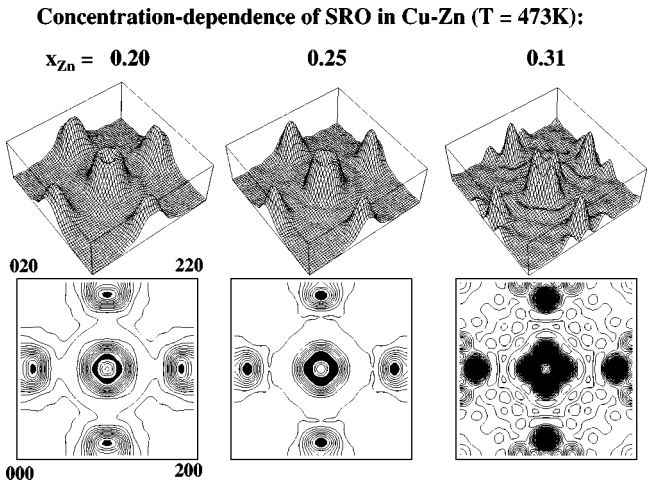

FIG. 9. SRO pattern and corresponding contour plot for Cu-Zn solid solutions with different concentrations.

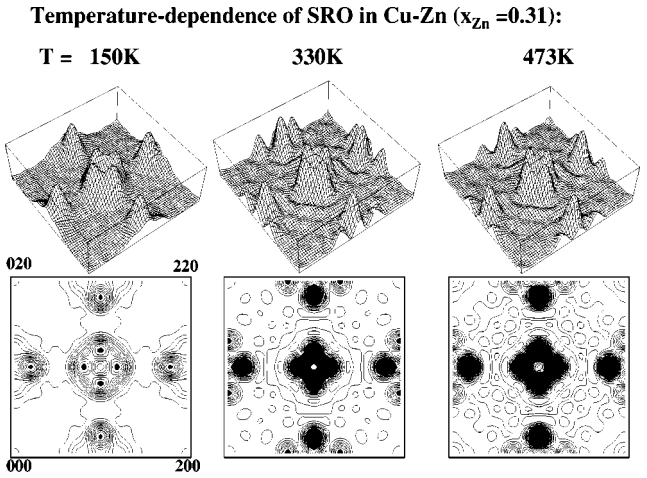

FIG. 10. SRO pattern and corresponding contour plot for α-brass above ($T=473$ K,330 K) and below ($T=150$ K) the critical temperature. The latter is the pattern of an ordered DO_{23} structure.

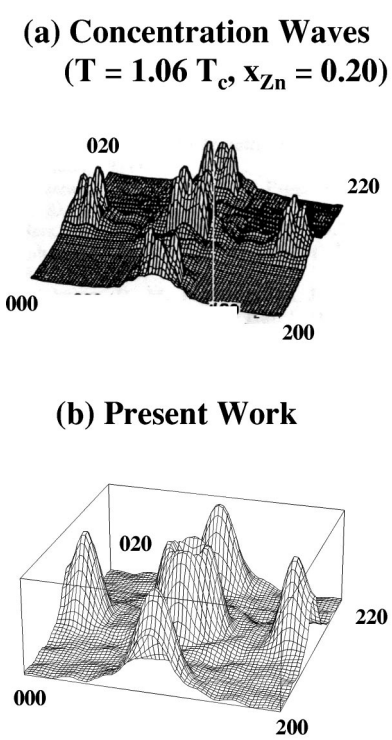

FIG. 11. Comparison of SRO pattern in α-brass resulting from (a) concentration waves (Ref. 21) and (b) this work.

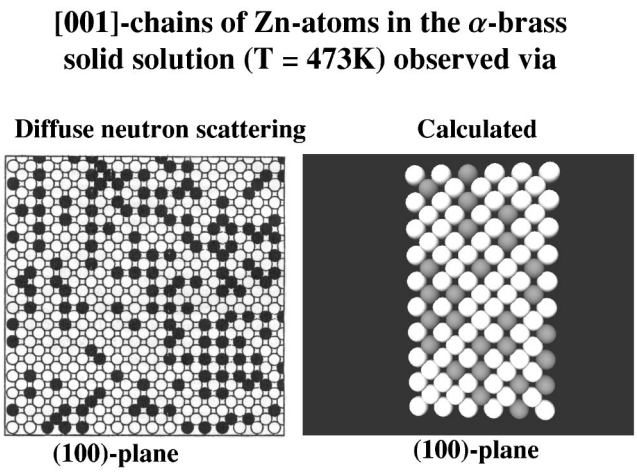

FIG. 12. Visualization of a (100) plane of α-brass (cut through the crystal) for $T=473$ K. While the left picture results from a model crystal based on diffuse neutron scattering experiments (Ref. 10), the right picture is the result of MC simulations using ΔH_{CE}. In both cases, chains of Zn atoms along [001] can be seen, indicating that SRO is present and, therefore, the observed solid solution cannot be described by a random alloy.

with that obtained from the Monte Carlo simulations of our LDA cluster expansion. Unlike our calculation, the pattern resulting from the concentration wave calculation shows a number of satellite spots around $\mathbf{k}=\langle 1\pm\epsilon,\ \sim\frac{1}{4},\ 0\rangle$ which might lead at low temperatures to ordering of a different structure than we find $(\mathrm{DO}_{23};M=2)$. Unfortunately, Turchi *et al.*[21] did not anneal their alloy in order to determine the corresponding ground-state structure, so a direct comparison with our predicted low-temperature phase is not possible.

F. Appearance of Zn chains in α-brass

Real-space imaging of the measured SRO in high-temperature quenched α-brass showed [001] chains of Zn atoms.[10] As discussed by Reinhard *et al.*,[10] these chains are a direct consequence of the observed SRO behavior of the system: While all SRO parameters described by $(lmn)=(2n;0;0)$ are positive (see Table III), all SRO parameters described by $(2n-1;1;0)$ are negative. This should lead to chains of Zn atoms along the [001] direction. The authors studied this assumption using an fcc model crystal which was fitted to the experimental SRO parameter of Table III. Figure 12 gives a comparison between the real-space structure deduced from experiment[10] and from our parameter-free model: In both cases, chains of Zn atoms are visible along [001], indicating that short-range order is essential for a quantitative correct description of the physical properties of the disordered solid solution of α-brass.

G. Effect of SRO on the mixing enthalpy

Figure 13 compares experimental mixing enthalpies as function of Zn concentration with earlier theoretical studies for the random alloy; i.e., no SRO is taken into account. The experimental values were taken from Ref. 4 and were measured at $T=773$ K. As discussed in the Introduction, Fig. 13

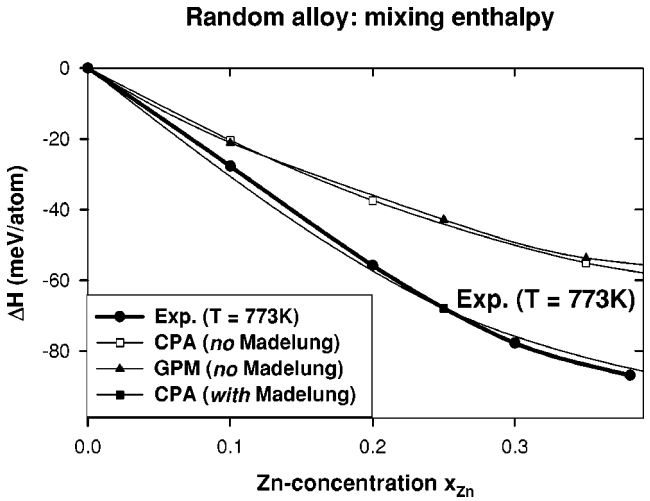

FIG. 13. Comparison of mixing enthalpies resulting from experiment (Ref. 4), GPM (Ref. 21), CPA without (Ref. 16), and with (Ref. 20) consideration of the Madelung energy.

clearly shows that charge transfer is making a big effect on the results. It can be seen that the corrected CPA of Johnson and Pinski[20] agrees very well with experiment, although SRO is neglected in the calculation. In order to study the influence of SRO on the mixing enthalpy, Fig. 14 compares $\Delta H_{mix}(x,T)$ for different temperatures, starting from the random alloy $(T\rightarrow\infty)$ and cooling down to temperatures where SRO sets in. Comparing the energy curves for the random and the disordered alloy, we see that the calculation neglecting SRO leads to much higher mixing enthalpies. Moreover, it can be seen that especially for higher Zn concentrations good agreement between experiment and calculated mixing enthalpies can only be reached, if SRO is taken into account. We do not have an explanation why the CPA calculations shown in Fig. 13 lead to reasonable mixing enthalpies without consideration of SRO.

The observed decrease of ΔH_{mix} with decreasing temperature can be discussed in terms of individual effective

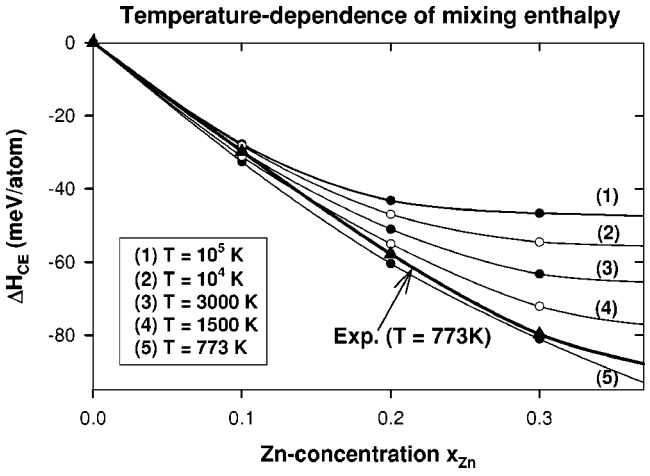

FIG. 14. Calculated mixing enthalpies of α-brass for different temperatures resulting from our MSCE and comparison with experimental value (Ref. 4).

TABLE IV. Correlation function of the first two nearest-neighbor interactions J_1, J_2, and of the four-atom interaction $J4$ for $x_{Zn}=0.3$ as function of temperature.

Temp. [K]	$\overline{\Pi}_1$	$\overline{\Pi}_2$	$\overline{\Pi}_{J4}$
100 000	0.157	0.161	0.003
100 00	0.133	0.170	−0.013
3000	0.095	0.202	−0.030
1500	0.059	0.258	0.060
773	0.017	0.366	−0.156

cluster interactions. For this purpose, we chose a concentration $x_{Zn}=0.3$ and study the contribution of each cluster probability $\overline{\Pi}_f$ as a function of temperature. Going back to Fig. 4(b), we see that the first pair interaction $J_1>0$ is ''antiferromagnetic'' (Cu-Zn attraction) while the second and third interactions $J_2, J_3<0$ are ''ferromagnetic'' (Cu-Zn repulsion). We find that the decrease in ΔH_{mix} with decreasing temperature is caused by the elimination of the first-neighbor pairs ($\overline{\Pi}_1 \rightarrow 0$) and enhancement of second-neighbor pairs ($\overline{\Pi}_2$ becomes more negative). This is shown in Table IV. Physically, this means that as the temperature is lowered, the alloy prefers to have unlike atoms as first nearest neighbor, and like atoms as second nearest neighbor. This automatically gives $L1_2$. Regarding multibody interactions, the most important contribution comes from the four-atom interaction $J4$ consisting of four nearest-neighbor atoms. Since $J4$ is positive (ordering is preferred), the change in the sign of $\overline{\Pi}_{J4}$ by lowering the temperature from $T=1500$ K to $T=773$ K (also shown in Table IV) leads to a strong decrease in ΔH_{mix}. Again, the negative sign of $J4 \cdot \overline{\Pi}_{J4}$ shows the tendency of forming $L1_2$ cells.

In summary, the alloy is stabilized at low temperatures by deviating systematically from randomness: It eliminates unlike-atom first-neighbor pairs and enhances unlike-atom second-neighbor pairs as well as tetrahedra made of unlike atoms.

H. Role of strain

Following the general statement that Cu-Zn is an ideal Hume-Rothery alloy,[11] strain should not play much of a role in the detailed description of the physical properties of the system. This assumption is supported by the small misfit between Cu and Zn (of about 4%) as well as by the qualitively successful descriptions of the solid solution using an unrelaxed random-alloy model[16,21] (see successful calculation of ΔH in Fig. 13). In this section we will test how far this approximation is justified for α-brass.

Figure 15 shows that the neglect of the constituent strain energy leads practically to complete, energetic degeneracy between $L1_2$, LPS_3, and DO_{23}. Although DO_{23} is still the lowest-energy structure, the difference between DO_{23} and $L1_2$ amounts to only about 0.1 meV/atom. The degeneration of $L1_2$, DO_{23}, and LPS3 means that the creation of periodic antiphase boundaries with modulation wavelengths $M=2$ and $M=3$ is only connected to extremely low-energy differences. Therefore, there exist a large number of excited states (in form of LPS with complex sequences of antiphase boundaries) being only about 0.1 meV/atom higher in energy than the true ground state DO_{23}. So the contribution of strain is, indeed, a stabilizing factor in order to get the correct ground state, but does not change the physics: Neglecting strain still leads to DO_{23} as ground state for Cu_3Zn.

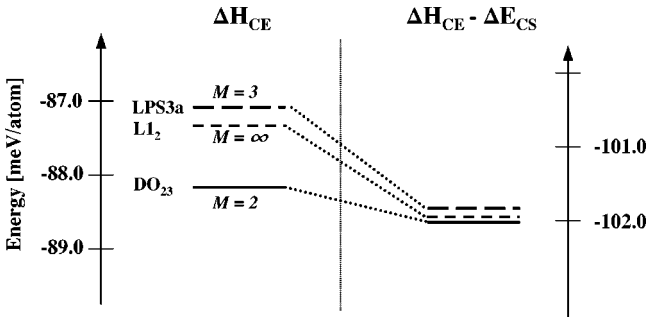

FIG. 15. Energy difference in the formation enthalpies of $L1_2$, DO_{23}, and LPS3 with and without taking the constituent strain energy into account.

Figure 16 shows ΔH_{CE} and $\Delta H_{CE}-E_{CS}$ for the random alloy ($T=100\,000$ K). The calculation with and without strain only leads to a small shift to lower energy values in the mixing enthalpies. The subtraction of the constituent strain energy was done *after* the Monte Carlo simulation, so that the difference between the two curves gives the magnitude of strain for the found equilibrium configuration as function of Zn concentration. We conclude that strain does not lead to qualitative changes in Cu-Zn.

IV. SUMMARY

We have used the MSCE approach to calculate from first principles the phase stability of α-brass. We find the following: (i) The low-temperature ordered phase is identified as the DO_{23} structure. (ii) The order-disorder transition tem-

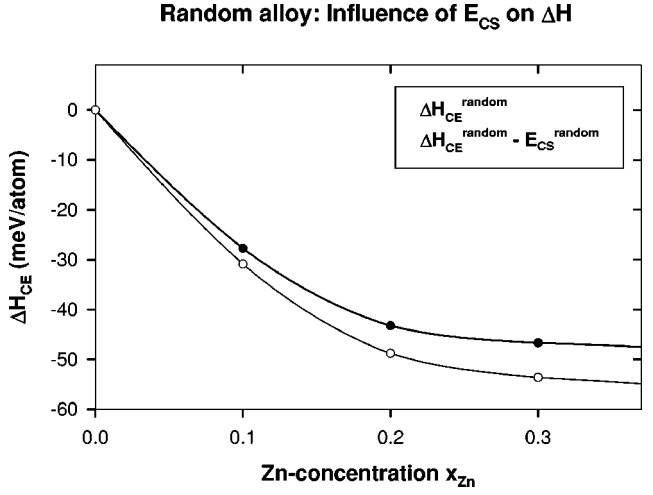

FIG. 16. Mixing enthalpy of the random alloy with (solid circles) and without (open circles) considering the constituent strain energy.

perature appears at relatively low temperatures which is probably the reason that the ordered structure was not yet detected experimentally: for $x_{Zn}=0.10$, $T_c=140$ K and for $x_{Zn}=0.33$, $T_c=295$ K. (iii) The high-temperature SRO scattering exhibits $\langle 1\frac{1}{4}0\rangle$ peaks, in close agreement with the neutron experiment of Reinhard *et al.*[10] (iv) In the disordered phase [001] chains of Zn atoms exist, as seen experimentally. (v) The calculated alloy mixing enthalpy with SRO is in close agreement with experiments, e.g., $\Delta H(x=0.3, T=773\ \mathrm{K})=-81.1$ meV/atom compared with the measured value of -77.8 meV/atom. (vi) The disordered alloy shows a temperature dependence: For a given concentration, the mixing enthalpy ΔH_{mix} becomes as more negative, as lower the temperature T; e.g., at $x_{Zn}=\Delta H_{mix}$ decreases from -54.6 meV/atom to -81.3 meV/atom as the temperature decreases form $T=100\,000$ K (random alloy) to $T=773$ K (disordered alloy). (vii) Neglect of strain leads to up to about 20% too low mixing enthalpies of the random alloy and to about 20 K too high critical temperatures.

Our theoretical study via LDA-based predictions on fcc-based Cu-Zn alloys shows that this system does not present a perfect random alloy: Neglect of short-range order leads, e.g., to much too small values for the mixing enthalpies of the solid solution. The ideal random alloy as a model to describe the physical properties of α-brass is also unable to explain experimental results, e.g., the appearance of [001] chains of Zn atoms as observed by neutron scattering experiments.[10]

ACKNOWLEDGMENTS

This work was supported by the Office of Science, Basic Energy Science, Material Science Division, U.S. Department of Energy under Contract No. DE-AC36-99-GO10337.

[1] L. Aitchison, *A History of Metals* (MacDonald and Evans Ltd., London, 1969).
[2] H.H. Coghlan, *Notes on the Prehistoric Metallurgy of Copper and Bronze in the Old World* (Oxford University Press, Oxford 1951).
[3] R.J. Forbes, *Metallurgy in Antiquity* (E.J. Brill, Leiden, 1950).
[4] R. Hultgren, P.D. Desai, D.T. Hawkins, M. Gleiser, and K.K. Kelley, *Selected Values of the Thermodynamic Properties of Binary Alloys* (American Society for Metals, Metal Park, OH, 1973).
[5] M. Ahlers, Prog. Mater. Sci. **30**, 135 (1986).
[6] W. Hume-Rothery, in *The Metallic State* (Oxford University Press, London, 1931).
[7] H.O. von Samson-Himmelstjerna, Z. Metallkd. **28**, 197 (1936).
[8] F. Körber and W. Oelsen, Mitt. K. W. Inst. Eisenforschung **19**, 209 (1937).
[9] F. Weibke, Z. Anorg. Allg. Chem. **232**, 289 (1937).
[10] L. Reinhard, B. Schönfeld, G. Kostorz, and W. Bührer, Phys. Rev. B **41**, 1727 (1990).
[11] T.B. Massalski and U. Mizutani, Prog. Mater. Sci. **22**, 151 (1978).
[12] Hiroshi Sato and Robert S. Toth, Phys. Rev. **124**, 1833 (1961).
[13] W. Adlassnig, W. Potzel, J. Moser, W. Schiessl, U. Potzel, C. Schäfer, M. Steiner, H. Karzel, M. Peter, and G.M. Kalvius, Phys. Rev. B **40**, 7469 (1989).
[14] M. Peter, W. Potzel, M. Steiner, C. Schäfer, H. Karzel, W. Schiessl, and G.M. Kalvius, Phys. Rev. B **47**, 753 (1993).
[15] D.D. Johnson, D.M. Nicholson, F.J. Pinski, B.L. Gyorffy, and G.M. Stocks, Phys. Rev. Lett. **56**, 2088 (1986).
[16] D.D. Johnson, D.M. Nicholson, F.J. Pinski, B.L. Gyorffy, and G.M. Stocks, Phys. Rev. B **41**, 9701 (1990).
[17] G.M. Stocks, W.M. Temmerman, and B.L. Gyorffy, Phys. Rev. Lett. **41**, 339 (1978).
[18] J.S. Faulkner and G.M. Stocks, Phys. Rev. B **23**, 5628 (1981).
[19] R. Magri, S.-H. Wei, and A. Zunger, Phys. Rev. B **42**, 11 388 (1990).
[20] D.D. Johnson and F.J. Pinski, Phys. Rev. B **48**, 11 553 (1993).
[21] P.E.A. Turchi, M. Sluiter, F.J. Pinski, D.D. Johnson, D.M. Nicholson, G.M. Stocks, and J.B. Staunton, Phys. Rev. Lett. **67**, 1779 (1991).
[22] P.E.A. Turchi, M. Sluiter, F.J. Pinski, D.D. Johnson, D.M. Nicholson, G.M. Stocks, and J.B. Staunton, Phys. Rev. Lett. **68**, 418(E) (1992).
[23] J.M. Sanchez, F. Ducastelle, and D. Gratias, Physica A **128**, 334 (1984).
[24] C. Wolverton, G. Ceder, D. de Fontaine, and H. Dreyssé, Phys. Rev. B **48**, 726 (1993).
[25] A. Zunger, *Statics and Dynamics of Alloy Phase Transformations*, Vol. 319 of *NATO Advanced Study Institute, Series B: Physics*, edited by P. E. A. Turchi and A. Gonis (Plenum Press, New York, 1994), p. 361.
[26] D.B. Laks, L.G. Ferreira, S. Froyen, and A. Zunger, Phys. Rev. B **46**, 12 587 (1992).
[27] In the past we showed that attenuation of E_{CS} was advantageous to better capture relaxation [C. Wolverton, V. Ozolins, and A. Zunger, J. Phys. C **12**, 2749 (2000)]. For Cu-Zn, the differences with and without attenuation are small, e.g., less than 3 meV/atom for the mixing enthalpies of the disordered alloy.
[28] Z.W. Lu, D.B. Laks, S.-H. Wei, and A. Zunger, Phys. Rev. B **50**, 6642 (1994).
[29] C. Wolverton, V. Ozoliņš, and A. Zunger, Phys. Rev. B **57**, 4332 (1998).
[30] J. Ihm, A. Zunger, and M.L. Cohen, J. Phys. C **12**, 4409 (1979).
[31] N. Troullier and J.L. Martins, Phys. Rev. B **43**, 1993 (1991).
[32] D.M. Ceperley and B.J. Alder, Phys. Rev. Lett. **45**, 566 (1980).
[33] J.P. Perdew and A. Zunger, Phys. Rev. B **23**, 5048 (1981).
[34] S. Froyen, Phys. Rev. B **39**, 3168 (1989).
[35] S. Müller, L.-W. Wang, and A. Zunger, C. Wolverton, Phys. Rev. B **60**, 16 448 (1999).
[36] Z.W. Lu, D.B. Laks, S.-H. Wei, and A. Zunger, Phys. Rev. B **50**, 6642 (1994).
[37] G. Ceder, D. de Fontaine, H. Dreysee, D.M. Nicholson, G.M. Stocks, and B.L. Gyorffy, Acta Metall. Mater. **38**, 2299 (1990).
[38] A. Zunger, S.-H. Wei, L.G. Ferreira, and J.E. Bernard, Phys. Rev. Lett. **65**, 353 (1990).